npj Science of Food

https://doi.org/10.1038/s41538-026-00723-9

Article in Press

From rosemary and coffee to bioactive nanovesicles: exploring new frontiers in food functional ingredients

Received: 25 July 2025

Accepted: 18 January 2026

Cite this article as: d'Adduzio, L., Aiello, G., Musazzi, U. *et al.* From rosemary and coffee to bioactive nanovesicles: exploring new frontiers in food functional ingredients. *npj Sci Food* (2026). https://doi.org/10.1038/s41538-026-00723-9

Lorenza d'Adduzio, Gilda Aiello, Umberto Musazzi, Carlotta Bollati, Giorgia Frigerio, Melissa Fanzaga, Maria Silvia Musco & Carmen Lammi

From Rosemary and Coffee to Bioactive Nanovesicles: Exploring New Frontiers in Food Functional Ingredients.

Lorenza d'Adduzio[1], Gilda Aiello[2], Umberto Musazzi[1], Carlotta Bollati[1], Giorgia Frigerio[1], Melissa Fanzaga[1], Maria Silvia Musco[1], Carmen Lammi[1]*

1. Department of Pharmaceutical Sciences, University of Milan, Milan, Italy
2. Department of Human Science and Quality of Life Promotion, Telematic University San Raffaele, Rome, Italy

*Corresponding Author: Carmen Lammi, Department of Pharmaceutical Sciences, University of Milan, via Mangiagalli 25, 20133 Milan, Italy. E-Mail: carmen.lammi@unimi.it, tel.: +39 02-50319372.

Abstract

Plant-derived vesicles (PDVs) are lipid-membrane structures that enclose proteins, lipids, nucleic acids and metabolites, reflecting the phytochemical profile of their plant source. This study investigated PDVs from *Rosmarinus officinalis* leaves (RVs) and *Coffea arabica* powder (CVs), isolated using a patented method. A multidisciplinary and multi-omic approach was employed to characterize their physico-chemical properties, metabolic and lipid profiles, and *in vitro* biological activities using fibroblasts (BJ-T5A) and myotubes (C2C12). RVs yield showed a higher vesicles concentration, with 1.37×10^{12} nanovesicle/mL, compared to 1.74×10^{10} nanovesicles/mL for CVs. RVs were found to be rich in diterpenes, flavonoids, and free fatty acids, while CVs contained chlorogenic and phenolic acids with higher lipid diversity, mainly diacylglycerols. Both RVs and CVs exhibited a defined morphology and showed strong antioxidant activity, reducing reactive oxygen species (ROS) and malondialdehyde (MDA) production in both cell models. Additionally, they enhanced collagen production and secretion in fibroblasts and positively modulated molecular targets related to fatty acid synthesis and glucose transport in myotubes. These findings support the potential of PDVs as natural delivery systems with beneficial properties in muscle health and tissue function.

Keywords: food bioactive, plant derived nanovesicles, plant extracts, C2C12 cells, human fibroblasts.

Introduction

Rosmarinus officinalis L. and *Coffea arabica* L. are rich sources of bioactive compounds with antioxidant and anti-inflammatory properties (1,2). Thus, rosemary and coffee extracts are usually employed in nutraceutical field, to counteract oxidative stress (3), and in cosmetics, since coffee shows skin toning and anti-aging effects, while rosemary enhances microcirculation and exhibits purifying activity (4,5). *Rosmarinus officinalis* extracts are commonly prepared from dried and fresh rosemary leaves and contain a wealth of polyphenolic compounds, including phenolic acids, flavonoids, and phenolic terpenes (6). While numerous antioxidant compounds contribute to the extracts' properties, the predominant ones, phenolic diterpenes, carnosic acid, and carnosol, account for over 90% of its antioxidant activity (7). The antioxidant properties of coffee stem from its content of chlorogenic, ferulic, caffeic, and n-coumaric acids (8). Interestingly, compounds formed during roasting process, such as the Maillard reaction products (e.g. melanoidins) are also known to exhibit radical scavenging and metal chelating properties, contributing to the overall antioxidant activity of the roasted coffee (9–11). The quality and value of commercial rosemary extracts are strongly influenced by their phenolic composition, especially the presence of carnosic acid and rosmarinic acid, which are the most abundant components and are well known for their diverse biological activities (12). Also in coffee extracts, preserve the phenolic content (mostly chlorogenic and caffeic acid content) is crucial to guarantee the extract's biological properties. Several studies report that the plant extracts' composition varies depending on the extraction method used. Different techniques can be applied to recover antioxidant phenolic compounds from natural sources, including solid-liquid extraction with organic solvents, ultrasound-assisted extraction, microwave-assisted extraction, supercritical fluids extraction and high-pressure processes (13,14). The extraction of bioactive compounds from medicinal plants or food matrices is commonly performed using solvent-based techniques (15,16), which often result in crude, chemically heterogeneous mixtures which are sensitive to degradative phenomena, such as temperature, pH, light and oxidation (17). As a result, conventional extraction methods frequently lead to the partial degradation or loss of active compounds, such as polyphenols, terpenoids, or alkaloids, reducing both their stability and bioactivity. Thus, novel encapsulation strategies (e.g. liposomes, synthetic nanoparticles) have been emerged to formulate plant extracts, protect them from degradation and delivering them safely with enhanced efficacy. In this context, naturally

plant-derived vesicles (PDVs) are nano-sized, lipid bilayer-bound structures that carry lipid, proteins, genetic material (miRNAs and DNA) and secondary metabolites, being naturally bio-formulated carriers of bioactive compounds. PDVs represent an emerging topic in the food science field that attracted increasing scientific interest due to their structural similarity to extracellular vesicles of mammalian and plant origin, their ability to protect their cargo and be uptaken at cellular level (18,19) and their biological properties showed both *in vitro* and *in vivo* (20–23). However, to date, despite their relevance as natural delivery systems of bioactives, a significant gap exists regarding their functional roles and biological implications in human health, probably due to the absence of an efficient standardized protocol for PDVs obtaining from different food matrixes. The mostly applied PDVs isolation approach is based on differential ultracentrifugation techniques that have some drawbacks, such as low recovery rates, low yield, being highly time consuming (24). Consequently, to address current limitations in PDVs isolation, we have recently developed and patented a reproducible method (International Publication Number WO 2024/223549 A1, licensed to Plantech s.r.l.) for obtaining, isolating and storing PDVs while maintaining their morphology, integrity, physicochemical properties, and bioactive components. In light with this information, by applying the patented methods, the aim of this study is to provide evidence regarding PDVs obtained from *Coffea arabica* powder (CVs) and *Rosmarinus officinalis* leaves (RVs). Their structural and physicochemical characteristics were investigated using nanoparticle tracking analysis (NTA), dynamic light scattering (DLS), and cryo-electron microscopy (Cryo-EM). To further elucidate their composition, metabolomic and lipidomic analyses were performed. Finally, the biological activities of CVs and RVs were then evaluated in human fibroblasts (BJ-5TA) and differentiated murine myotubes (C2C12), two cell type that dynamically interplay in maintaining and restoring the skeletal muscle health. More in detail, we focused on CVs and RVs antioxidant properties in both cell lines (25,26). Specifically, we assessed their ability to reduce reactive oxygen species (ROS) and malondialdehyde (MDA) production, along with their influence on key molecular pathways involved in oxidative stress, collagen production in fibroblasts, and intracellular fatty acid and glucose metabolisms in myotubes, respectively.

Results

RVs and CVs production and chemical characterization

To assess the morphology of CVs and RVs, Cryo-EM analysis was conducted and revealed differences between the two vesicle preparations. CVs (Figure 1A) appeared as an aggregate of round, electron-dense structures surrounded by a diffuse halo, possibly indicating the presence of loosely packed lipidic material or debris. The main structure displayed sensitivity to beam exposure, meaning that under the electron beam the vesicles rapidly lost contrast and definition. This behaviour is typically observed for lipid-rich or poorly ordered materials, which are prone to radiation damage and structural disruption during imaging. Such beam sensitivity supports the hypothesis that the CVs contain loosely packed or amorphous lipid components (27,28). In contrast, RVs (Figure 1B) exhibited a cleaner background with more defined, uniformly sized round vesicles dispersed across the field of view. The overall morphology of RVs was consistent with intact lipid bilayer vesicles, indicating better preservation and structural integrity.

DLS and NTA analysis were employed to characterize the size distribution, polydispersity, and concentration RVs and CVs (Figure 1 C and Table 1). Figure 1C confirmed the presence of nanoparticles in both samples, with a main population peaking between 100 and 150 nm for both CVs and RVs, a size range typical of nanovesicles. However, RVs showed a markedly higher particle concentration compared to CVs. This difference suggests a higher yield or better recovery efficiency for RVs. In addition, at a scattering angle of 173°, CVs exhibited a hydrodynamic diameter (Dh) of 300 nm with a polydispersity index (PDI) of 0.351, indicating moderate heterogeneity. RVs showed a smaller Dh of 222 nm but a higher PDI of 0.479, suggesting greater size dispersion. At 12.8°, both samples presented significantly larger Dh values (593 nm for CVs and 565 nm for RVs), likely due to the detection of larger aggregates or broader particle distributions. Notably, CVs displayed a markedly high PDI at this angle (0.923), supporting the presence of a heterogeneous and potentially aggregated vesicles population. The derived count rate (DCR) was consistently higher in RVs across both angles, reaching 16,702 kcps at 173°, in contrast to 5,473 kcps for CVs, indicating a greater number of scattering particles in the rosemary-derived vesicles sample. NTA analysis further confirmed these observations (Table 1). RVs showed a significantly higher particle concentration, with 1.37×10^{12} particles/mL, compared to 1.74×10^{10} particles/mL for CVs. The median particle size (D50) was comparable between the two samples (159.2 nm for CVs and 156.1 nm for RVs), although CVs displayed a slightly broader

distribution, as reflected by higher D90 values (277 nm vs. 268.9 nm). Overall, RVs demonstrated a more uniform size distribution, higher particle yield, and greater colloidal stability compared to CVs.

Secondary metabolite profile in CVs and RVs

The untargeted metabolomic profiling of vesicles isolated from coffee powder and rosemary leaves (Tables S1 and S2) revealed distinct yet complementary phytochemical encapsulations, each reflective of their botanical origin. Coffee-derived vesicles were predominantly enriched in chlorogenic acids, including cryptochlorogenic, 3,4-dicaffeoylquinic, and 4,5-dicaffeoylquinic acids, as well as phenolic acids (caffeic, ferulic, protocatechuic) and organic acids (citric, quinic, malic, succinic), reflecting a metabolic signature primarily associated with antioxidant potential. Rosemary-derived vesicles exhibited a broader biochemical composition, notably housing diterpenes such as carnosic acid and carnosol, alongside rosmarinic acid, additional phenolic acids (caffeic, vanillic, p-coumaric), an array of flavonoids (apigenin, diosmetin, wogonin, hesperetin, kaempferol), triterpenoids (betulinic, betulonic acids), proteinogenic amino acids (e.g., L-glutamic acid, L-tryptophan), and nucleosides (guanosine). This broader chemical diversity observed in rosemary-derived vesicles, particularly concerning flavonoids and terpenoids, contrasts with the chlorogenic acid-rich profile of coffee-derived vesicles. These differences in metabolite composition are ~~clearly~~ observable in the heatmap (Figure 2) and may reflect distinct phytochemical loading mechanisms or botanical specificity in vesicle cargo enrichment.

Lipidic profile in CVs and CVs

High-resolution HPLC-MS analysis of plant-derived nanovesicles from Rosmarinus and Coffea revealed divergent lipidomic architectures and class-specific distributions (Tables S3 and S4). In rosemary-derived nanovesicles, the lipidome was dominated by free fatty acids (FAs), which accounted for approximately 75% of the total lipid species detected. These included a wide range of saturated and monounsaturated FAs (e.g., FA 14:0 to FA 36:0), as well as polyunsaturated species such as FA 18:5 and FA 32:4, suggesting the presence of plant-derived ω-3 analogues. Diacylglycerols (DGs) contributed to 10%, with DG 32:0 and DG 36:9 as major constituents, while triacylglycerols (TGs) and N-acylethanolamines (NAEs) represented ~8% and ~5%, respectively. Minor lipid classes such as lysophosphatidylcholine (LPC), lysophosphatidylglycerol (LPG), and

phosphatidylglycerol (PG) made up less than 2% of the total. Conversely, coffee-derived nanovesicles exhibited greater lipid diversity and a lipidome skewed toward neutral lipids. Diacylglycerols (DGs) represented the dominant class (~40%), encompassing a wide array of molecular species, including DG 22:1 to DG 44:6. Free fatty acids constituted 25%, with several long-chain saturated and monounsaturated species. Triacylglycerols (TGs) were present at higher levels (15%) than in rosemary and included highly extended forms such as TG 64:0 and TG 66:0. Notably, monoacylglycerols (MGs) and phosphatidylcholines (PCs), which were not detected in rosemary vesicles, collectively contributed ~8%, while NAEs, ceramides, and phytosterols together accounted for the remaining ~7%.

CVs and RVs antioxidant activity evaluation on fibroblasts and myotubes.

To exclude any cytotoxic effects, MTT assays were performed on fibroblasts BJ-5TA and myotubes C2C12. The cells were treated with CVs and RVs at 7.8×10^6nanovesicles/ml, 39×10^6 nanovesicles/ml and 78×10^6nanoveislces/ml (corresponding to 0.1, 0.5 and 1 mg nanovesicles/mL) for 48 hours, respectively. The results (Figure S1) show the absence of negative effects on cells viability in both cell lines. Considering the MTT results and the phytochemical profile of CVs and RVs, we investigated their antioxidant properties at cellular level by evaluating their impact on ROS and MDA production in both BJ-5TA and differentiated C2C12 cells. To evaluate whether the samples modulate the H_2O_2-induced ROS production, BJ-5TA and C2C12 cells were pre-treated with RVs and CVs (7.8×10^6 nanovesicles/mL and 39×10^6 nanovesicles/mL) overnight. The following day, C2C12 cells were treated with H_2O_2 20 μM and BJ-T5A with 200 μM, respectively, to induce the oxidative stress. Figure 3 A and C ~~clearly~~ suggest that the treatment of cells with H_2O_2 alone produces a significant augmentation of intracellular ROS levels by 406±3.06% in fibroblasts and 1408±27.2% in myotubes cells versus the control cells, which was attenuated by the RVs and CVs pre-treatment that reduced the H_2O_2 induced intracellular ROS. In particular, RVs ($7,8 \times10^6$ nanovesicles/mL and 39×10^6 nanovesicles/mL) reduced ROS production up to 366±14,534% and 358,7 ±0,863% in fibroblast and 1256±2.026% and 1181±11,76 in myotubes; CVs ($7,8 \times10^6$nanovesicles/mL and 39×10^6nanovesicles/mL) reduce ROS production up to 302.4±4.878% and 279±06.853% in fibroblast and 1105±9.749% and 1084±13.91% in myotubes, respectively, confirming that it can act as a natural antioxidant (Figure 3 A and C).

Cellular membrane lipids are susceptible to oxidative damage, primarily by ROS, leading to a specific chain reaction that produces end products such as MDA and its related compounds, collectively referred to as TBA reactive substances. Considering these observations, the effectiveness of RVs and CVs in modulating H_2O_2-induced lipid peroxidation in fibroblasts and myotubes was evaluated. This evaluation involved measuring the reaction between the precursor of MDA and the TBA reagent to generate a fluorometric product (with excitation wavelength λ_{ex} = 532 nm and emission wavelength λ_{em} = 553 nm), which is indicative of the quantity of TBARS (MDA present). In agreement with the observed increase of ROS after the H_2O_2 treatment, a significant increase of the lipid peroxidation was observed up to 121.2±0.9574% and 126.7±1.976% at cellular level in fibroblasts and myotubes, respectively. In addition, the pre-treatment of both the cell lines with all the samples determined a significant reduction of lipid peroxidation. Figure 3 B and C ~~clearly~~ shows that the MDA production was attenuated by the pre-treatment with RVs and CVs. In particular, RVs (7,8 x10^6nanovesicles/mL and 39 x10^6nanovesicles/mL) reduced MDA production up to 105.8±1.880% and 99.05±5.387% in fibroblast and up to 101.9±1.47% and 92.52±1.51 in myotubes; CVs (7.8 x 10^6 nanovesicles/mL and 39 x 10^6 nanovesicles/mL) reduced MDA production up to 88.92±9.622% and 91.04±6.557% in fibroblast and up to 94.42±2.92% and 81.58±4.24% in myotubes, respectively (Figure 3, B and D). Since the lipid peroxidation is a validated marker of oxidative stress, these findings confirm the effective antioxidant nanovesicles property reducing intracellular MDA production.

Molecular effects of RVs and CVs on oxidative stress and cellular energy balance pathways in differentiated C2C12 cells

Myotubes and fibroblasts are key players in muscle and connective tissue repair. Fibroblasts produce ECM components like collagen, while myotubes regenerate muscle, thus their interactions can influence tissue remodelling. Differentiated C2C12 cells that forming contractile myotubes and producing characteristic muscle proteins were employed for studying oxidative stress, fatigue, and recovery mechanisms relevant to muscle health. In light of these evidences, considering the strong antioxidant effects of rosemary and coffee nanovesicles, we investigated the effect of RVs and CVs (39x10^6 nanovesicles/mL) on cellular target involved in oxidative stress (nuclear factor erythroid 2-related factor 2, NRF2) and inflammatory (cyclooxygenase-2, COX-2) responses, lipid metabolism (fatty acid synthase, FASN, and lipid accumulation) and glucose homeostasis

(transporter protein type-4, GLUT4) in C2C12 cells. Our findings indicated that after the treatment of C2C12 cells with H_2O_2 20 μM, a significant decrease of Nrf-2 protein level by 59.35 ±17.8% was observed versus control cells (Figure 4A). The pre-treatment with RVs and CVs showed antioxidant activity through the Nrf-2 pathway modulation in H_2O_2 treated C2C12 cells. In facts, RVs and CVs ($39x10^6$ nanovesicles/mL) increased the Nrf-2 protein levels up to 107.5 ±18.56% and 138.0 ±42.25%, respectively. Figure 3 B indicates that after the treatment of C2C12 cells with H_2O_2 (20 μM), a significant increase of COX-2 protein level by 123.2 ±14.48% was observed versus control cells. Interestingly, the both RVs and CVs pretreatments modulate COX-2 expression in H_2O_2 treated C2C12 cells. In facts, RVs and CVs ($39x10^6$ nanovesicles/mL) decreased the COX-2 protein levels up to 77.29±13.36% and 61.51 ±22.39%, respectively (Figure 4 B). Both RVs and CVs positively impact on protein levels of pAMPK, the phosphorylated (active) form of AMPK, an energy sensor kinase that is activated when cellular ATP levels are low by promoting catabolic pathways like glucose uptake and fatty acid oxidation and restoring energy balance (29). Oxidative stress (H_2O_2 20 μM) decreased the protein level expression of pAMPK 84.50±6.44%, the RVs and CVs pretreatments at $39x10^6$ vesicles/mL, increased the pAMPK protein level expression up to 131.43±10.49% and 138.4±6.77%, respectively (Figure 5 A and B). Consequently, FASN and GLUT4 protein levels were also modulated in differentiated C2C12 cells. Indeed, as shown in Figure 4 C, while oxidative stress induced using H_2O_2 at 20 μM, increased the FASN protein levels up to 135.9±4.07%, RVs and CVs ($39x10^6$ vesicles/mL) decreased the FASN protein levels up to 94.11±14.86% and 79.13 ±9.47%, respectively. Lastly, oxidative stress (H_2O_2 20 μM) decreased the GLUT4 protein levels up to 75.8±14.57%, RVs and CVs (39x106 vesicles/mL) increased the GLUT4 protein levels up to 134.7±7.024% and 258.7 ±16.297%, respectively.

In addition, the lipid accumulation in differentiated C2C12 cells was induced by H_2O_2 that significantly increased the relative lipid content up to 123±8.33% (Figure 5 D). The treatment with RVs and CVs restored the relative lipid content up to 83.86±17.32 and 71.44±15.40%.

RVs and CVs improve the collagen and elastin homeostasis in human fibroblasts.

Fibroblasts are distributed throughout the body's connective tissues, where they produce an extracellular matrix primarily composed of type I and type III collagen and elastin (30). In response to tissue injury, nearby fibroblasts proliferate, migrate to the wound site, and secrete large

quantities of collagen-rich matrix. This process plays a key role in isolating and repairing the damaged tissue, contributing to give structure and elasticity. The oxidative stress induces a marked reduction in the synthesis of collagen and secretion of both collagen and elastin, with important implications for tissue integrity and function (31). To investigate the ability of RVs and CVs to exert beneficial effects on human fibroblasts, Western blot experiments were conducted by analysing the variation in collagen production after 24 h from the pretreatment with RVs and CVs. In particular, the oxidative stress induces a reduction in collagen protein synthesis up to 54.63±4.860% (Figure 6 A). Interestingly, the RVs and CVs pretreatments ($39x10^6$ nanovesicles/mL) led to an increase of protein levels up to 118.4±2.60%. for RVs and 150.5±2.61% for CVs, respectively (Figure 6 A).

The impact of RVs and CVs treatment on extracellular matrix stability was investigated by ELISA assays on H_2O_2 aged fibroblasts supernatants by evaluating collagen and elastin secretion. The results in Figure 6 B and C ~~clearly~~ demonstrate that H_2O_2 alone reduces the collagen and elastin secretion up to 89.18±3.060% and 81.31±3.579% respectively. On contrary, the RVs and CVs pretreatments (7.8 and $39x10^6$ nanovesicles/mL) induced a significant dose dependent increase of collagen secretion up to 106.5±7.479% and 125.4±1.428%, and 119.9±0,476% and 123.2±2.040 %, respectively. Importantly, the RVs and CVs pretreatments at the same concentrations, induced a comparable significant increase of elastin secretion up to 104.5±12.43% and 111.3±4.33%, and 110.8±0.50% and 112.7±0.94%, respectively. Since collagen and elastin are important in maintaining the ECM structure, these results clearly suggest that RVs and CVs actively contribute to positively impact on ECM maintaining.

Discussion

The cryo-EM analysis (Figure 1 A and B) revealed morphological differences CVs and RVs. CVs appeared as aggregates of electron-dense particles surrounded by a diffuse halo, likely indicating loosely packed lipids or debris, and showed sensitivity to the electron beam, suggesting structural fragility. In contrast, RVs displayed uniformly sized, round vesicles with well-defined edges and a clean background, consistent with intact lipid bilayer structures. DLS measurements in Table 1 showed that RVs had a smaller hydrodynamic diameter (222 nm) but higher polydispersity, while CVs were larger (300 nm) with moderate heterogeneity. At lower scattering angles, both samples showed increased size due to aggregates, with CVs being more affected. The derived count rate and NTA results indicated a significantly higher particle concentration in RVs (1.37×10^{12}

nanovesicles/mL) compared to CVs (1.74×10^{10} nanovesicles/mL). RVs also had a narrower size distribution and greater colloidal stability. These results suggest that both the food matrices can be employed for PDVs obtaining and that the proposed technology is more effective and yields better-quality plant vesicles from the rosemary leaves than from the coffee powder. Several bioactive metabolites identified in CVs and RVs are well-documented for their antioxidant and anti-inflammatory activities, largely mediated through direct scavenging of ROS and the modulation of redox-sensitive signalling pathways. Therefore, the RVs and CVs antioxidant properties were investigated on fibroblasts and myotubes, two cellular type that crosstalk in preserving muscle functionality, since myotubes contribute to muscle regeneration and fibroblasts regulate the extracellular environment, being the cell type of the muscle connective tissue (39). Under oxidative stress condition, fibroblasts undergo molecular alterations that impair collagen synthesis, promote senescence, and disrupt extracellular matrix homeostasis (40,41). In myotubes, oxidative stress is one of the major contributors to fatigue and muscle injury associated with physiological aging or high-intensity exercise (42). Interestingly, CVs and RVs reduced ROS and MDA production in both fibroblasts and myotubes stimulated with H_2O_2, with CVs that demonstrated to be more antioxidant when tested at equal number of nanovesicles/mL (Figure 3). On myotubes, the antioxidant activity of CVs and RVs was deeply investigated at molecular level, where both the samples demonstrated to positively affect in a comparable way the protein level expression of Nrf2 and COX-2 (Figure 3). The strong antioxidant properties of CVs and RVs can be attributed to their richness in phytochemicals, mainly represented by chlorogenic acids, including cryptochlorogenic, 3,4-dicaffeoylquinic, and 4,5-dicaffeoylquinic acids, as well as phenolic acids (caffeic, ferulic, protocatechuic) and organic acids (citric, quinic, malic, succinic) in CVs, and diterpenes such as carnosic acid and carnosol, rosmarinic acid, additional phenolic acids (caffeic, vanillic, p-coumaric), flavonoids (apigenin, diosmetin, wogonin, hesperetin, kaempferol), triterpenoids (betulinic, betulonic acids), proteinogenic amino acids (e.g., L-glutamic acid, L-tryptophan) in RVs. In rosemary, the diterpenes carnosic acid, carnosol, have been consistently shown to exert strong antioxidant and anti-inflammatory effects. Specifically, carnosic acid and carnosol scavenge ROS both directly and by activating endogenous antioxidant systems via the Nrf2 pathway. They also suppress inflammatory responses by modulating NF-κB, MAPK, and NLRP3 inflammasome signalling, thereby reducing levels of TNF-α, IL-1β, and COX-2 (43,44). Rosmarinic acid contributes significantly to antioxidant defense by scavenging free radicals and

suppressing the production of nitric oxide and superoxide production in activated macrophages. It inhibited inducible nitric oxide synthase (iNOS) and suppressed Iκ-Bα phosphorylation, suggesting a role in inhibiting both ROS and inflammatory signaling pathways (45). Although less extensively studied in rosemary, flavonoids such as apigenin, diosmetin, and wogonin also play an important role. Apigenin, for instance, has been shown to reduce oxidative stress and inflammation through inhibition of COX-2, NF-κB, and STAT3 pathways, and by modulating mitochondrial ROS production (46,47). In CVs, the phenolic compounds chlorogenic acids (including cryptochlorogenic acid and dicaffeoylquinic acid isomers) represent the dominant antioxidant species. Additionally, chlorogenic acids mitigate oxidative stress by inhibiting ROS generation and suppressing pro-inflammatory cytokines such as IL-6 and TNF-α, particularly in LPS-stimulated macrophages (48,49), and via modulation of NF-κB and Nrf2 signalling pathways (50). Taken together, both RVs and CVs carry phytochemicals capable of mitigating oxidative stress and inflammation. Importantly, our results suggest that the biological properties of CVs and RVs exceeded the antioxidant activity. RVs and CVs' whole phytochemicals and lipid content may exert a synergic activity that led to distinct molecular effects in fibroblasts and myotubes. In fibroblasts, the treatment with CV and RVs induced an upregulation of collagen synthesis, in parallel with an increase of collagen and elastin secretion (Figure 6), indicating their potential role in ECM homeostasis maintenance. Among the most significant metabolites identified, caffeic acid, rosmarinic acid, p-coumaric acid, and vanillic acid, contribute to protecting fibroblasts from oxidative damage and have been implicated in modulating signalling pathways such as TGF-β, which directly influence collagen biosynthesis (51). Rosmarinic acid is of particular interest due to its dual origin from both the phenylpropanoid and shikimate pathways. It exhibits both antioxidant and anti-inflammatory properties, which help maintain ECM integrity and support collagen stabilization under stress conditions. Flavonoids such as apigenin, luteolin, and kaempferol also detected in both rosemary and, to a lesser extent, coffee, are known inhibitors of collagen-degrading enzymes such as collagenase, thereby indirectly preserving collagen structure. Their additional antioxidant and anti-inflammatory effects further support fibroblast activity and ECM homeostasis (52). Lastly, L-glutamic acid, L-aspartic acid, and L-alanine, ubiquitous amino acids found in both species, serve as fundamental building blocks in protein metabolism, including collagen production, although their effects are likely supportive rather than regulatory. Indeed, several lipids identified in RVs and CVs exhibit the potential to enhance collagen synthesis and

elastin secretion in aged human dermal fibroblasts. Notably, ceramides such as Cer 40:1;O3, found in CVs, have been shown to promote the expression of collagen and fibrillin through the activation of TGF-β and FGF2 signalling pathways, thereby improving skin elasticity and counteracting dermal aging (53). NEAs, including NAE 14:0, 18:0, and 18:1, present in both RVs and CVs, exert anti-inflammatory effects and contribute to extracellular matrix homeostasis, suggesting an indirect yet supportive role in collagen regulation (54). Additionally, saturated fatty acids such as FA 16:0 and FA 18:0, although not directly implicated in collagen biosynthesis, support membrane structure and cellular stability in fibroblasts (55), while structural phospholipids such as PC, LPC, and PG further contribute to membrane integrity and cellular signalling. These findings reinforce the potential utility of both CVs and RVs in applications aimed at enhancing ECM integrity, highlighting ceramides and NAEs as key bioactive lipids in RVs and CVs with the most compelling evidence for enhancing the regenerative capacity of aged tissues. Importantly, NAEs and ceramides may also modulate oxidative and inflammatory pathways through NRF2 and COX-2 regulation (56). In differentiated C2C12 myotubes pretreated with lipid-rich nanovesicles, enhanced NRF2 activation and reduced COX-2 expression were observed, indicating a dual antioxidant and anti-inflammatory effect that could synergistically support ECM remodelling and fibroblast function.

In myotubes, RVs and CVs activate the AMPK signalling pathway, as shown by increased pAMPK levels, leading to the downregulation of FASN and upregulation of GLUT4, suggesting a shift toward improved metabolic regulation and energy homeostasis (Figure 5 A, B and C). From a functional point of view, the downregulation of FASN was translated in a reduction of the lipid accumulation in myotubes (Figure 5 D). AMPK is a potent metabolic regulator and plays an important role in various metabolic pathways, such as lipid and glucose metabolism (57,58). Its activation reflects an adaptive response to cellular energy stress that promotes GLUT4 expression and translocation, enhancing glucose uptake for ATP production via glycolysis. Interestingly, the concurrent upregulation of FASN may suggest a compensatory mechanism to support lipid remodelling or energy storage. The coordinated modulation of glucose and lipid pathways contributes to restoring energy homeostasis under oxidative or metabolic stress. Previous studies demonstrated that rosmarinic acids promoted energy expenditure associated with up-regulating genes and proteins related to energy expenditure in skeletal muscle cells and carnosic acid from rosemary extract stimulates skeletal muscle cell glucose uptake via AMPK activation (59,60).

Among the phytochemicals identified in CVs, caffeic acid methyl ester and caffeic acid ethyl ester, which can be formed during the metabolism or thermal processing of coffee, have been shown to promote GLUT4 translocation in skeletal muscle cells via an insulin-independent pathway that activates AMPK, enhancing glucose uptake even in the absence of insulin stimulation (61). These findings suggest that caffeic acid esters may mimic exercise-like metabolic activity, a property highly desirable for managing insulin resistance. Similarly, ferulic acid and its derivatives, present in roasted coffee as breakdown products of chlorogenic acids, exhibit strong antioxidant activity and are known to influence glucose metabolism through redox-sensitive signaling cascades. Although direct evidence for GLUT4 activation is more limited, their structural similarity and shared metabolic pathways with caffeic acid support a possible synergistic effect on GLUT4 expression (62). Chlorogenic acids and their derivatives, such as dicaffeoylquinic acids, have been shown to enhance glucose uptake by upregulating GLUT4 expression and promoting its translocation (63,64). Among flavonoids, luteolin has shown promise in prior literature for enhancing GLUT4 expression via AMPK and PI3K/Akt pathways. Luteolin co-presence in coffee alongside caffeic acid and chlorogenic acid derivatives supports its inclusion as a candidate with potential additive effects. In contrast, methylxanthines such as theophylline, while abundant in coffee, may exert inhibitory effects on GLUT4 activity. Theophylline has been reported to interfere with insulin signalling by inhibiting PI3K activity, thereby potentially reducing insulin-stimulated GLUT4 translocation (65). These opposing mechanisms highlight the complexity of coffee's metabolic impact and suggest that the net effect on GLUT4 activity may depend on the balance of stimulatory and inhibitory compounds, as well as individual metabolic context. Taking all the results into account and comparing the bioactivity of both RVs and CV, it is evident that coffee derived nanovesicles are more effective in counteracting energy metabolism impairment and oxidative stress in muscle cell, as well as in supporting collagen biosynthesis in stressed fibroblasts. In conclusion, the present study demonstrates that plant-derived vesicles obtained from rosemary leaves and coffee powder are a promising and multifaceted strategy for the targeted delivery of bioactive molecules endowed with strong antioxidant properties. Notably, PDVs demonstrated to be naturally bioformulated nanocarriers enriched in metabolites that did not show any cytotoxic effects *in vitro*, confirming their safety and biocompatibility at the cellular level. In this framework, PDVs offer an innovative and advanced delivery platform that might significantly enhance the bioactivity and functional impact of phytocomplexes, thereby potentially overcoming

key limitations associated with conventional plant extracts. To achieve this overall goal further investigation will be performed for assessing the stability and structural integrity of both RVs and CVs over the time, as important features that can ensure their bioactivity.

Methods

Chemicals

All chemicals and reagents were of analytical grade and from commercial sources. Hydrochloric acid (HCl) 3-(4,5-dimethylthiazol-2-yl)-2,5- diphenyltetrazolium bromide (MTT), ROS and lipid peroxidantion (MDA) assay kits were from Sigma- Aldrich (St. Louis, MO, USA). Dulbecco's modified Eagle medium (DMEM), fetal bovine serum (FBS), L- glutamine, phosphate buffered saline (PBS), penicillin/streptomycin, 24 and 96- well plates were from Euroclone (Milan, Italy). NaOH, RIPA buffer, protease inhibitor cocktail, PMSF, Na-or-thovanadate, Bovine serum albumin (BSA) and the antibody against β-actin were bought from Sigma-Aldrich (St. Louis, MO, US). Dulbecco's modified Eagle's medium (DMEM), L-glutamine, fetal bovine serum (FBS), phosphate buffered saline (PBS), penicillin/streptomycin, chemiluminescent reagent, dry milk powder and multi-well plates were purchased from Euroclone (Milan, Italy). Mini protean TGX pre-cast gel 7.5% and Mini nitrocellulose Transfer Packs were purchased from BioRad (Hercules, CA, US). ELISA kit and antibody against COL1A1 (Collagen alpha 1(I) chain) and ELN (Elastin) were from Proteintech (Rosemont, USA). 10 kDa molecular weight cut-off Amicon® Ultra and horse serum were from Sigma-Aldrich (St. Louis, MO, US). Antibodies against rabbit Ig-horseradish peroxidase (HRP) and mouse Ig-HRP were purchased from Santa Cruz Biotechnology Inc. (Santa Cruz, CA, USA). The antibody against Phospho-AMPKα (Thr172) (4188) and GLUT-4 (2213) were from Cell Signaling Technology (Danvers, Massachusetts, USA). The antibody against Collagen Type I (Cat No. 66761-1-Ig) and Fatty Acis Synthase (FASN, Cat No. 10624-2-AP), COX2/ Cyclooxygenase 2 (Cat No. 12375-1-AP) and nuclear factor erythroid 2-related factor 2 (NRF2) (Cat No. 66504-1-Ig) were from Proteintech.

RVs and CVs obtaining, isolation and purification

To obtaining CVs and RVs, commercially and food grade available coffee powder (50g) and rosemary leaves (50g) were macerated, separately, at 4°C overnight in 1:1 Tris-HCl 20 mM pH 7.2. The day after, the samples were separately homogenized keeping the sample as cool as

possible to avoid the matrix degradation and encourage the vesicles formation through the membranes' rearrangement. The homogenates were sieved to recover the liquid filtrate.

After the sieving step, CVs and RVs were isolated and purified by differential centrifugation followed by ultrafiltration (UF) step respectively. More in detail, the homogenates obtained were subjected to sequential differential centrifugation to remove large debris and plant material at 700g × 10 minutes at 4°C. The pellet was discarded, and the supernatant collected for the next centrifugation step at 700g × 10 minutes at 4°C. The pellet was discarded, and the supernatant collected for the next centrifugation step at 1500g × 20 minutes at 4°C. The pellet was discarded, and the supernatant collected for the next centrifugation step at 3000g×30 minutes at 4°C. The pellet was discarded, and the supernatant was collected. The supernatant was ultra-filtrated by a filter device (Amicon® Ultra 100K device — 10,000 MWCO) applying a centrifuge at 4000g × 30' at 4°C. The retentate were discarded and the filtrate kept for the following analysis.

Nanoparticle Tracking Analysis (NTA)

Particle size distribution and concentration were analyzed by a nanoparticle tracking analysis (NTA) using a NanoSight NS300 (Malvern Panalytical, Malvern, UK) equipped with a blue laser (404 nm, 70 mV) and sCMOS camera. Before the analysis, the samples were diluted in HPLC-grade water to reach the ideal particle concentration range in terms of particles/frame (20–120 particles/frame). Temperature was held constant at 25 °C during the experiment, and for each sample, five 60 s videos were recorded and, subsequently, analyzed using NTA software 3.0 (NanoSight, Malvern Panalytical, Malvern, UK).

Dynamic Light Scattering

The Z-average diameter (D_h) and the polydispersity index (PDI) of samples were evaluated by photon correlation spectroscopy using a dynamic light scatter (DLS, Zetasizer Nano ZS, Malvern Instrument, Malvern, UK), equipped with a backscattered light detector, operating at dual angle (173°, 12.8°) mode and at 25 °C. Before the analysis, the samples were diluted in HPLC-grade water to reach the ideal particle concentration range. The results calculated using the Dispersion Technology Software (Malvern Instruments, Malvern, UK) are reported as intensity distribution.

Morphological analysis by cryogenic electron microscopy (Cryo-EM)

Samples vitrification was performed using a Mark IV Vitrobot (Thermo Fisher Scientific). A 3 µl aliquot of the sample was applied to either Quantifoil R 2/1 Cu 300-mesh grids or Lacey carbon grids, both of which had been glow-discharged at 30 mA for 30 seconds using a GloQube system (Quorum Technologies). Immediately after application, the grids were blotted in a climate-controlled chamber at 4 °C and 100% humidity, followed by plunge-freezing into liquid ethane. Vitrified grids were transferred to a Talos Arctica transmission electron microscope (Thermo Fisher Scientific) operating at 200 kV and equipped with a Ceta 16M detector (Thermo Fisher Scientific). Images were acquired at nominal magnifications ranging from 22,000x to 45,000x, corresponding to pixel sizes of 4.66 Å/pixel and 2.29 Å/pixel, respectively. All cryo-EM experiments were conducted at the NoLimits center, University of Milan.

Metabolomics

All samples have been analyzed at UNITECH OMICs (University of Milano, Italy) using the ExionLC™ AD system (SCIEX connected ZenoTOF 7600 System (SCIEX) equipped with Turbo V™ Ion Source with ESI Probe. Samples were separated on CORTECS UPLC T3 (1.6 µm, 2.1x150 mm) (Waters™) using mobile phase A (0.1% formic acid in water) and mobile phase B (0.1% formic acid in acetonitrile) at a flow rate of 400 µL/min. The chromatographic gradient was performed at a constant flow rate of 400 µL/min. From 0.00 to 2.00 minutes, the mobile phase composition was held at 99% solvent A and 1% solvent B. Between 2.00 and 6.00 minutes, the same composition was maintained. From 6.00 to 10.00 minutes, a linear gradient was applied to reach 75% solvent A and 25% solvent B. Between 10.00 and 15.00 minutes, the gradient continued to reach 5% solvent A and 95% solvent B. At 15.20 minutes, the composition was returned to the initial condition of 99% solvent A and 1% solvent B. The run was stopped at 20.00 minutes. The column and autosampler temperatures were set at 40°C and 10°C, respectively. The sample injection volume was 5 µL. MS spectra were collected over an m/z range of 50-1500 Da in negative polarity, operating in IDA®mode (Information Dependent Acquisition). The collision energy was set at 30 (CES 15). The data was processed using SCIEX OS ver 3.0 (SCIEX)™ software integrated with LibraryView ver 1.4, a database (Natural Products HR-MS/MS Library) containing more than 1000 MS/MS spectra and Formula Finder, an algorithm that tries to predict the possible chemical formula based on the MS spectrum, using the accuracy of mass of the precursor ion and the isotopic pattern. The analytes were identified by comparing the MS/MS

spectra obtained and those reported in the databases consulted. A "non-targeted screening workflow" was also carried out to verify the presence of additional analytes not present in the database, by assigning a brute formula.

Lipid Extraction by MTBE

The lipids extraction was performed on 50 µL of resuspended pellet using the standard MTBE protocol, with MTBE/methanol/water (10:3:2.5, v/v/v) as the extraction solvent ratio [12]. All solvents contained BHT 0.1% w/v to prevent unwanted oxidation. Briefly, 375 µL of MeOH was added to each sample and vortexed for 5 s. Then, 1250 µL of MTBE were added, followed by 5 s of vortexing and incubation (1 h, 4 °C, and 210 rpm). The phase separation was induced by adding 315 µL of H_2O, followed by 5 s of vortexing for 5 s and 10 min of incubation (4 °C and 210 rpm). Once centrifugated (4 °C, 10 min, and 2000× g), the upper phase was collected into a new tube. The re-extraction was performed through 323 µL MTBE, 96.8 µL MeOH, and 80.7 µL H20 (all spiked with 0.1% w/v BHT in H20) followed by centrifugation (4 °C, 10 min, and 2000× g). The upper phases were pulled together and dried under vacuum (Eppendorf concentrator 5301, 1 mbar). Before the LC-MS analyses, lipid extracts were dissolved in 100 µLi-PrOH and vortexed.

Mass Spectrometry for Untargeted Analysis of Lipidome

All samples have been analyzed at UNITECH OMICs (University of Milano, Italy) using an ExionLC™ AD system (SCIEX) connected to a TripleTOF™ 6600 System (SCIEX) equipped with a Turbo V™ Ion Source and an ESI Probe. Chromato-graphic separation was achieved on a Kinetex® EVO C18 (Phenomenex) 100 (Length) × 2.1 mm (ID) × 1.7 µm (Particle Size) using mobile phase A (H_2O/ACN (60/40, v/v, with ammonium acetate 10 mM and 0.1% formic acid) and mobile phase B (i-PrOH/ACN (90/10, v/v, with ammonium acetate 10 mM and 0.1% formic acid) at a flow rate of 400 µL/min. The column and temperatures were set at 45 °C. The sample injection volume was 5 µL. The elution gradient was set as below follows: 0–2 min (45% B), 2–12 min (45–97% B), 12–17 min (97% B), 17–17.10 min (97–45% B), and 17.10–20 min (45% B). MS spectra were collected over an m/z range of 140–1500 Da, operating in IDA mode (Information-Dependent Acquisition). Collision energy was set at to 35 (CES 15) (p. Polarity: positive/negative). Three technical replicates (LC-MS/MS runs) were performed. Raw LC-HRMS files of all samples were first imported into MS-DIAL 4.8

(http://prime.psc.riken.jp/compms/msdial/main.html, 1st April 2023), followed by manual annotation and integration,) for peak detection, deconvolution, and alignment. A linear-weighted moving average was used as the default for peak detection to accurately determine the left- and right edges of the peak. The next step matched features with the integrated MS2 spectral Lipidblast database using the corresponding predicted fragment ions in MS-DIAL. MS1 and MS2 tolerance were fixed at 0.01 Da and 0.025 Da, respectively. To avoid false positives, the identification score cut-off was set at to 80%. Peak intensities were aligned across. The retention time tolerance was fixed at 0.05 min with MS1 tolerance at 0.015 Da. The carry-over was controlled by regularly measured blank samples. Unknown entries were removed from the identifications.

Cell culture and differentiation

hTERT-immortalized human skin fibroblasts BJ-5TA cell line was bought from ATCC (ATCC (CRL-4001 ™), from LGC Standards, Milan, Italy), cultured in DMEM high glucose and Medium 199 (4:1 ratio) with stable L-glutamine supplemented with 10% FBS, 100 U/mL penicillin, 100 µg/mL streptomycin and incubated at 37 ◦C under a 5% CO_2 atmosphere. Mouse myoblast (C1C12 cells) were sourced bought from ATCC (HB-8065, ATCC from LGC Standards, Milan, Italy). Cells were regularly sub-cultured using a previously optimized protocol (66). The culture medium consisted of DMEM containing 25 mM glucose, 3.7 g/L of $NaHCO_3$, 4 mM of stable L-glutamine, 1% non-essential amino acids, 100 U/L of penicillin, and 100 µg/L of streptomycin (complete medium), plus 10% heat-inactivated FBS. The cells were kept at 37°C in a 5% CO_2 atmosphere. For C2C12 cells differentiation, the differentiation medium consisted of DMEM containing 25 mM glucose, 3.7 g/L of $NaHCO_3$, 4 mM of stable L-glutamine, 1% non-essential amino acids, 100 U/L of penicillin, and 100 µg/L of streptomycin (complete medium), plus 2% heat-inactivated horse serum (67).

3-(4,5-Dimethylthiazol-2-yl)-2,5-Diphenyltetrazolium Bromide (MTT) Assay

1×10^4 BJ-5TA cells or C2C12 cells/well were seeded in 96-well plates, and after 24 hours, the cells were treated with vehicle or RVs or CVs 7.8, 39 and 78×10^6 vesicles/mL (corresponding to 0.1, 0.5 and 1 mg nanovesicles/mL) in complete growth media for 48 hours at 37 °C in an environment containing 5% CO_2. Following aspiration of the treatment, 100 µL/well of filtered 3-(4,5-dimethylthiazol-2-yl)-2,5-diphenyltetrazolium bromide (MTT) solution was applied. Following a two-hour incubation period at 37 °C with 5% CO_2, 100 µL/well of the lysis buffer (8 mM HCl + 0.5% NP-40 in DMSO) was added after aspirating the 0.5 mg/mL solution. The absorbance at 575 nm was measured on the Synergy H1 fluorescence plate reader (Biotek, Bad Friedrichshall, Germany) after 10 minutes of gentle shaking.

Fluorometric intracellular ROS assay

A black 96-well plate was used to 1×10^4 cells/well BJ-5TA cells and C2C12 cells in growth media, and the cells were left there overnight. After removing the medium the next day, each well was filled with 50 µL of Master Reaction Mix and 50 µL of full DMEM. The cells were then incubated for an hour at 37 °C and 5% CO_2 in the dark. Cells were then treated with RVs and CVs

7.8 and 39 $\times 10^6$ vesicles/mL (corresponding to 0.1 and 0.5 mg nanovesicles/mL) and incubated for a full day at 37 °C. Reactive oxygen species (ROS) were generated by exposing cells to 1.0 mM H_2O_2 for 60 minutes at 37 °C in the absence of light. Following that, fluorescence signals (ex./em. 490/525 nm) were captured using a Biotek Synergy H1 microplate reader.

Lipid Peroxidation (MDA) Assay

BJ-5TA (2.5×10^5 cells/well) and C2C12 cells (1.5×10^5 cells/well) were grown in a 24-well plate and then RVs or CVs 7.8 and 39×10^6 vesicles/mL (corresponding to 0.1 and 0.5 mg nanovesicles/mL), for 24 hours at 37 °C in 5% CO_2 atmosphere. Following an hour of incubation with either vehicle (H_2O) or H_2O_2 at a concentration of 1 mM, the cells were harvested and homogenized in 150 µL of ice-cold MDA lysis solution containing 3 µL of butylated hydroxytoluene (BHT). After centrifuging the samples at 13,000 g for 10 minutes, 300 µL of the TBA solution was added to each vial holding 100 µL of samples to create the MDA-TBA adduct. After 60 minutes of incubation at 95 °C, the vials were allowed to cool to room temperature in ice for ten minutes. For measurement, 100 µL of each reaction mixture were pipetted into a clear 96-well plate. At 532 nm, the absorbance was determined using the Biotek Synergy H1 microplate reader.

Western blot analysis

Western blot experiments have been performed using conditions previously optimized (68). Briefly, BJ-5TA cells/well (1.1×10^5 cells/well 24-well plate) and C2C12 cells (75×10^3 cells/well 24-well plate) were treated with RVs or CVs 39×10^6 vesicles/mL (corresponding to 0.1 and 0.5 mg nanovesicles/mL), for 24 h. After each treatment, cells were scraped in 30 µL ice-cold lysis buffer [RIPA buffer + inhibitor cocktail + 1:100 PMSF + 1:100 Na-orthovanadate] and transferred in an ice-cold microcentrifuge tube. After centrifugation at 13,300g for 15 min at 4 °C, the supernatant was recovered and transferred into a new ice-cold tube. Total proteins were quantified by Bradford method and 50 µg of total proteins loaded on a pre-cast 7.5% Sodium Dodecyl Sulfate - Polyacrylamide (SDS-PAGE) gel at 130 V for 45 min. Subsequently, the gel was pre-equilibrated with 0.04% SDS in H2O for 15 min at RT and transferred to a nitrocellulose membrane (Mini nitrocellulose Transfer Packs,) using a trans-Blot Turbo at 1.3 A, 25 V for 7 min. Target proteins, on milk or BSA blocked membrane, were detected by primary antibodies against COX-2, Nrf2,

pAMPK, GLUT4, FASN and β-actin, In particular, on Secondary antibodies conjugated with HRP and a chemiluminescent reagent were used to visualize target proteins and their signal was quantified using the Image Lab Software (Biorad). The internal control β-actin was used to normalize loading variations.

Enzyme-linked immunosorbent assay (ELISA)

Collagen and elastin levels in cell culture supernatants were quantified using the AuthentiKine ELISA kit (Proteintech), following the manufacturer's instructions. Briefly, supernatants collected from treated and H_2O_2-stimulated BJ-5ta cells were first centrifuged at 15,000 × g for 10 minutes at 4 °C to remove cellular debris and insoluble material. The resulting supernatants were then used for the assay. For each sample, 100 µL was added to the wells of the ELISA plate, which was incubated for 2 hours at room temperature (RT). After incubation, the wells were emptied and washed four times with 250 µL of Wash Buffer. Subsequently, 100 µL of the Conjugate Solution was added to each well, followed by a further 2-hour incubation at RT. The wells were then washed again four times with Wash Buffer before adding 100 µL of Substrate Solution. The plate was incubated in the dark at RT until a blue colour developed. The enzymatic reaction was then stopped by adding 50 µL of Stop Solution, and absorbance was measured at 450 and 540 nm using a Synergy H1 plate reader (BioTek Instruments).

Oil Red O staining

C2C12 cells (1×10^5) were seeded in 96-well plate and kept in complete growth medium for 24 hours. After 24 hours, cells were treated with RVs and CVs 7.8 and 39×10^6 vesicles/mL (corresponding to 0.1 and 0.5 mg nanovesicles/mL), for 24 hours. To induce lipid accumulation, the day after, C2C12 cells were treated with H_2O_2 20 µM overnight. After the incubation time, the medium was removed, C2C12 cells were washed three times with PBS to remove unbound staining and fixed with 10% formalin for 1 h. After washing for three times with distilled water, cells were washed with 60% isopropanol briefly and incubated with 60% filtered Oil Red for 1 hour to stain the adipocytes. Then, the staining was removed, and cells were washed twice with PBS. Since the

Oil red O solution has been used to stain the adipocytes, the absorbance at 490–520 nm was measured using the Synergy H1 absorbance plate reader from Biotek.

Statical Analysis

All measurements were performed in triplicate and results were expressed as the mean ± standard deviation (s.d.), where p-values < 0.05 were considered to be significant. Statistical analyses were performed by ONE and 2way ANOVA followed by Dunnett's and Tukey's post-test (Graphpad Prism 9, GraphPad Software, La Jolla, CA, USA).

Data availability: Data will be available on specific request to the authors.

Supplementary Material: Supplementary Material provides the Figure 1S: MTT results and Tables S1, S2, S3 and S4.

Acknowledgement

We acknowledge UNITECH OMICs, mass spectrometry platform of Università degli Studi di Milano, for running mass spectrometry analyses. We are indebted to Carlo Sirtori Foundation (Milan, Italy) for having provided part of equipment used in this experimentation. The method described in this paper, which includes RVs and CVs isolation, purification and stabilization is referenced in the patent WO 2024/223549 A1 (Method for the production of plant-derived nanovesicles and their applications) and licensed to Plantech srl (Italy).

Author Contribution: Conceptualization C.L.; methodology L.d'A., G.A., U.M., G.F., G.A., M.F., C.B. ; formal analysis L.d'A., G.A., M.F., C.B., M.S.M; resources C.L.; data curation: L.d'A., G.A., M.F., C.B.; supervision: C.L. writing L.d'A., G.A., C.L.—original draft preparation and review. All authors have read and agreed to the published version of the manuscript.

Conflict of Interest

Authors declare no conflict of interest.

Figure Captions:

Figure 1 – **Cryogenic electron microscopy of CVs and RVs**. (A) Coffee-derived vesicles. (B) Rosemary-derived vesicles. Scale bar 50 nm for both the pictures. (C) NTA of CVs and RVs samples, respectively.

Figure 2 – **Hierarchical clustering heatmaps of the relative abundance of common phytochemicals (one-way ANOVA and post-hoc analysis, $p < 0.05$) of CVs and RVs**. More expressed phytochemicals are indicated in red, with intensity values represented by colored cells (red for higher expression and dark blue for lower expression); the samples are shown in the rows, and the features are shown in the columns.

Figure 3 – RVs and CVs antioxidant activity. Evaluation of the effects of the RVs and CVs on H_2O_2 -induced reactive oxygen species (ROS) and MDA production levels in fibroblast BJ-5TA cells (A, B) and differentiated C2C12 (C, D) cells. The data points represent the averages ± SD of three independent experiments in duplicate. All data sets were analyzed by one-way ANOVA followed by Tukey's post hoc test. Different lowercase letters indicate a significant difference ($p < 0.05$) between different treatments. Control: untreated cells. RVs: rosemary vesicles; CVs: coffee vesicles. 7.8×10^6 vesicles/mL and 39×10^6 vesicles/mL correspond to 0.1 and 0.5 mg nanovesicles/mL.

Figure 4 – Nrf2 and COX-2 protein levels in C2C12 cells pretreated with RVs and CVs $39x10^6$ vesicles/mL in oxidative stress induced damage. The data points represent the averages ± SD of three independent experiments in duplicate. All data sets were analyzed by one-way ANOVA followed by Tukey's post hoc test. Different lowercase letters indicate a significant difference ($p < 0.05$) between different treatments. Control: untreated cells. RVs: rosemary-derived vesicles; CVs: coffee-derived vesicles. 7.8×10^6 vesicles/mL and 39×10^6 vesicles/mL correspond to 0.1 and 0.5 mg nanovesicles/mL.

Figure 5 – pAMPK, FASN and GLUT4 protein levels and quantification of intracellular lipid accumulation in C2C12 cells pretreated with RVs and CVs $39x10^6$ vesicles/mL in oxidative

stress induced damage. The data points represent the averages ± SD of three independent experiments in duplicate. All data sets were analysed by one-way ANOVA followed by Tukey's post hoc test. Different lowercase letters indicate a significant difference ($p < 0.05$) between different treatments. Control: untreated cells. RVs: rosemary-derived vesicles; CVs: coffee-derived vesicles. pAMPK: AMP-activated protein kinase; GLUT-4: Glucose Transporter; FASN: Fatty Acid Synthase. 7.8×10^6 vesicles/mL and 39×10^6 vesicles/mL correspond to 0.1 and 0.5 mg nanovesicles/mL.

Figure 6 – Impact of CVs and RVs on collagen synthesis and collagen and elastin extracellular release. Collagen protein levels (A) and collagen and elastin secretion in human fibroblasts pretreated with RVs and CVs $39x10^6$ nanovesicles/mL in oxidative stress induced damage (B, C). The data points represent the averages ± SD of three independent experiments in duplicate. All data sets were analyzed by one-way ANOVA followed by Tukey's post hoc test. Different lowercase letters indicate a significant difference ($p < 0.05$) between different treatments. Control: untreated cells. RVs rosemary-derived vesicles; CVs: coffee-derived vesicles. 7.8×10^6 vesicles/mL and 39×10^6 vesicles/mL correspond to 0.1 and 0.5 mg nanovesicles/mL.

References

1. Borrás-Linares I, Stojanović Z, Quirantes-Piné R, Arráez-Román D, Švarc-Gajić J, Fernández-Gutiérrez A, et al. Rosmarinus Officinalis Leaves as a Natural Source of Bioactive Compounds. Int J Mol Sci. 2014 Nov 10;15(11):20585–606.
2. Vignoli JA, Viegas MC, Bassoli DG, Benassi M de T. Roasting process affects differently the bioactive compounds and the antioxidant activity of arabica and robusta coffees. Food Research International. 2014 Jul;61:279–85.
3. Saeed M, Naveed M, BiBi J, Ali Kamboh A, Phil L, Chao S. Potential nutraceutical and food additive properties and risks of coffee: a comprehensive overview. Crit Rev Food Sci Nutr. 2019 Nov 13;59(20):3293–319.
4. Alu'datt MH, Rababah T, Alhamad MN, Gammoh S, Al-Mahasneh MA, Tranchant CC, et al. Pharmaceutical, Nutraceutical and Therapeutic Properties of Selected Wild Medicinal Plants: Thyme, Spearmint, and Rosemary. In: Therapeutic, Probiotic, and Unconventional Foods. Elsevier; 2018. p. 275–90.
5. Blanco-Llamero C, Macário HF, Guedes BN, Fathi F, Oliveira MBPP, Souto EB. Bioactives in Nutricosmetics: A Focus on Caffeine from Tea to Coffee. Cosmetics. 2024 Aug 28;11(5):149.
6. Mena P, Cirlini M, Tassotti M, Herrlinger K, Dall'Asta C, Del Rio D. Phytochemical Profiling of Flavonoids, Phenolic Acids, Terpenoids, and Volatile Fraction of a Rosemary (Rosmarinus officinalis L.) Extract. Molecules. 2016 Nov 19;21(11):1576.
7. Senanayake SPJN. Rosemary extract as a natural source of bioactive compounds. Journal of Food Bioactives. 2018 Jun;51–7.
8. Nicoli MC, Anese M, Manzocco L, Lerici CR. Antioxidant Properties of Coffee Brews in Relation to the Roasting Degree. LWT - Food Science and Technology. 1997 May;30(3):292–7.
9. Yashin A, Yashin Y, Wang J, Nemzer B. Antioxidant and Antiradical Activity of Coffee. Antioxidants. 2013 Oct 15;2(4):230–45.
10. del Castillo MD, Ames JM, Gordon MH. Effect of Roasting on the Antioxidant Activity of Coffee Brews. J Agric Food Chem. 2002 Jun 1;50(13):3698–703.
11. Farah A, De Paulis T, Moreira DP, Trugo LC, Martin PR. Chlorogenic acids and lactones in regular and water-decaffeinated arabica coffees. J Agric Food Chem. 2006;54(2).
12. Mulinacci N, Innocenti M, Bellumori M, Giaccherini C, Martini V, Michelozzi M. Storage method, drying processes and extraction procedures strongly affect the phenolic fraction of rosemary leaves: An HPLC/DAD/MS study. Talanta. 2011 Jul;85(1):167–76.
13. Markom M, Hasan M, Daud WRW, Singh H, Jahim JM. Extraction of hydrolysable tannins from Phyllanthus niruri Linn.: Effects of solvents and extraction methods. Sep Purif Technol. 2007 Jan 1;52(3):487–96.
14. Cortazar E, Bartolomé L, Delgado A, Etxebarria N, Fernández LA, Usobiaga A, et al. Optimisation of microwave-assisted extraction for the determination of nonylphenols and phthalate esters in sediment samples and comparison with pressurised solvent extraction. Anal Chim Acta. 2005 Apr 8;534(2):247–54.
15. Ivanović M, Islamčević Razboršek M, Kolar M. Innovative Extraction Techniques Using Deep Eutectic Solvents and Analytical Methods for the Isolation and Characterization of Natural Bioactive Compounds from Plant Material. Plants. 2020 Oct 24;9(11):1428.
16. Bhadange YA, Carpenter J, Saharan VK. A Comprehensive Review on Advanced Extraction Techniques for Retrieving Bioactive Components from Natural Sources. ACS Omega. 2024 Jul 23;9(29):31274–97.

17. Armendáriz-Barragán B, Zafar N, Badri W, Galindo-Rodríguez SA, Kabbaj D, Fessi H, et al. Plant extracts: from encapsulation to application. Expert Opin Drug Deliv. 2016 Aug 2;13(8):1165–75.
18. Wang B, Zhuang X, Deng Z Bin, Jiang H, Mu J, Wang Q, et al. Targeted drug delivery to intestinal macrophages by bioactive nanovesicles released from grapefruit. Molecular Therapy. 2014;22(3).
19. Raimondo S, Naselli F, Fontana S, Monteleone F, Lo Dico A, Saieva L, et al. Citrus limon-derived nanovesicles inhibit cancer cell proliferation and suppress CML xenograft growth by inducing TRAIL-mediated cell death. Oncotarget. 2015;6(23).
20. Yang M, Liu X, Luo Q, Xu L, Chen F. An efficient method to isolate lemon derived extracellular vesicles for gastric cancer therapy. J Nanobiotechnology. 2020 Dec 20;18(1):100.
21. Cai Y, Zhang L, Zhang Y, Lu R. Plant-Derived Exosomes as a Drug-Delivery Approach for the Treatment of Inflammatory Bowel Disease and Colitis-Associated Cancer. Pharmaceutics. 2022 Apr 8;14(4):822.
22. Raimondo S, Urzì O, Meraviglia S, Di Simone M, Corsale AM, Rabienezhad Ganji N, et al. Anti-inflammatory properties of lemon-derived extracellular vesicles are achieved through the inhibition of <scp>ERK</scp> / <scp>NF-κB</scp> signalling pathways. J Cell Mol Med. 2022 Aug 4;26(15):4195–209.
23. Yazdanpanah S, Romano S, Valentino A, Galderisi U, Peluso G, Calarco A. Plant-Derived Exosomes: Carriers and Cargo of Natural Bioactive Compounds: Emerging Functions and Applications in Human Health. Nanomaterials 2025, Vol 15, Page 1005 [Internet]. 2025 Jun 30 [cited 2025 Jul 25];15(13):1005. Available from: https://www.mdpi.com/2079-4991/15/13/1005/htm
24. Théry C, Witwer KW, Aikawa E, Alcaraz MJ, Anderson JD, Andriantsitohaina R, et al. Minimal information for studies of extracellular vesicles 2018 (MISEV2018): a position statement of the International Society for Extracellular Vesicles and update of the MISEV2014 guidelines. J Extracell Vesicles. 2018 Dec 23;7(1).
25. Böttcher N, Suhr F, Pufe T, Wruck CJ, Fragoulis A. Luteolin Induces Nrf2 Activity in C2C12 Cells: Implications for Muscle Health. Int J Mol Sci [Internet]. 2025 May 1 [cited 2025 Oct 27];26(9):4092. Available from: https://www.mdpi.com/1422-0067/26/9/4092/htm
26. Mendias CL. Fibroblasts take the centre stage in human skeletal muscle regeneration. J Physiol [Internet]. 2017 Aug 1 [cited 2025 Oct 27];595(15):5005. Available from: https://pmc.ncbi.nlm.nih.gov/articles/PMC5538237/
27. Sharma KD, Heberle FA, Waxham MN. Visualizing lipid membrane structure with cryo-EM: Past, present, and future. Emerg Top Life Sci [Internet]. 2023 [cited 2025 Oct 27];7(1):55. Available from: https://pmc.ncbi.nlm.nih.gov/articles/PMC10355340/
28. Shi D, Huang R. Analysis and comparison of electron radiation damage assessments in Cryo-EM by single particle analysis and micro-crystal electron diffraction. Front Mol Biosci. 2022 Oct 5;9:988928.
29. Garcia D, Shaw RJ. AMPK: Mechanisms of Cellular Energy Sensing and Restoration of Metabolic Balance. Mol Cell [Internet]. 2017 Jun 15 [cited 2025 Jul 24];66(6):789–800. Available from: https://www.cell.com/action/showFullText?pii=S1097276517303969
30. Mackey AL, Magnan M, Chazaud B, Kjaer M. Human skeletal muscle fibroblasts stimulate *in vitro* myogenesis and *in vivo* muscle regeneration. J Physiol. 2017 Aug 23;595(15):5115–27.

31. Sephel GC, Davidson JM. Elastin Production in Human Skin Fibroblast Cultures and Its Decline with Age. Journal of Investigative Dermatology. 1986 Mar;86(3):279–85.
32. Baldini N, Torreggiani E, Roncuzzi L, Perut F, Zini N, Avnet S. Exosome-like Nanovesicles Isolated from Citrus limon L. Exert Antioxidative Effect. Curr Pharm Biotechnol. 2018;19(11).
33. Berger E, Colosetti P, Jalabert A, Meugnier E, Wiklander OPB, Jouhet J, et al. Use of Nanovesicles from Orange Juice to Reverse Diet-Induced Gut Modifications in Diet-Induced Obese Mice. Mol Ther Methods Clin Dev. 2020;18.
34. Zhuang X, Deng Z Bin, Mu J, Zhang L, Yan J, Miller D, et al. Ginger-derived nanoparticles protect against alcohol-induced liver damage. J Extracell Vesicles. 2015;4(1).
35. Sánchez-López CM, Manzaneque-López MC, Pérez-Bermúdez P, Soler C, Marcilla A. Characterization and bioactivity of extracellular vesicles isolated from pomegranate. Food Funct. 2022;13(24):12870–82.
36. Liu H, Song J, Zhou L, Peng S, McClements DJ, Liu W. Construction of curcumin-fortified juices using their self-derived extracellular vesicles as natural delivery systems: grape, tomato, and orange juices. Food Funct. 2023;14(20):9364–76.
37. Kilasoniya A, Garaeva L, Shtam T, Spitsyna A, Putevich E, Moreno-Chamba B, et al. Potential of Plant Exosome Vesicles from Grapefruit (Citrus × paradisi) and Tomato (Solanum lycopersicum) Juices as Functional Ingredients and Targeted Drug Delivery Vehicles. Antioxidants. 2023 Apr 17;12(4):943.
38. Arslan D, Musa Özcan M. Evaluation of drying methods with respect to drying kinetics, mineral content and colour characteristics of rosemary leaves. Energy Convers Manag. 2008 May;49(5):1258–64.
39. Mackey AL, Magnan M, Chazaud B, Kjaer M. Human skeletal muscle fibroblasts stimulate *in vitro* myogenesis and *in vivo* muscle regeneration. J Physiol. 2017 Aug 23;595(15):5115–27.
40. Fisher GJ, Quan T, Purohit T, Shao Y, Cho MK, He T, et al. Collagen Fragmentation Promotes Oxidative Stress and Elevates Matrix Metalloproteinase-1 in Fibroblasts in Aged Human Skin. Am J Pathol. 2009 Jan;174(1):101–14.
41. Martins SG, Zilhão R, Thorsteinsdóttir S, Carlos AR. Linking Oxidative Stress and DNA Damage to Changes in the Expression of Extracellular Matrix Components. Front Genet. 2021 Jul 29;12.
42. Lian D, Chen MM, Wu H, Deng S, Hu X. The Role of Oxidative Stress in Skeletal Muscle Myogenesis and Muscle Disease. Antioxidants. 2022 Apr 11;11(4):755.
43. Habtemariam S. Anti-Inflammatory Therapeutic Mechanisms of Natural Products: Insight from Rosemary Diterpenes, Carnosic Acid and Carnosol. Biomedicines. 2023 Feb 13;11(2):545.
44. Satoh T, Trudler D, Oh CK, Lipton SA. Potential Therapeutic Use of the Rosemary Diterpene Carnosic Acid for Alzheimer's Disease, Parkinson's Disease, and Long-COVID through NRF2 Activation to Counteract the NLRP3 Inflammasome. Antioxidants. 2022 Jan 6;11(1):124.
45. Qiao S, Li W, Tsubouchi R, Haneda M, Murakami K, Takeuchi F, et al. Rosmarinic acid inhibits the formation of reactive oxygen and nitrogen species in RAW264.7 macrophages. Free Radic Res. 2005 Sep 7;39(9):995–1003.
46. Ai XY, Qin Y, Liu HJ, Cui ZH, Li M, Yang JH, et al. Apigenin inhibits colonic inflammation and tumorigenesis by suppressing STAT3-NF-κB signaling. Oncotarget. 2017 Nov 21;8(59):100216–26.

47. Duarte S, Arango D, Parihar A, Hamel P, Yasmeen R, Doseff A. Apigenin Protects Endothelial Cells from Lipopolysaccharide (LPS)-Induced Inflammation by Decreasing Caspase-3 Activation and Modulating Mitochondrial Function. Int J Mol Sci. 2013 Aug 28;14(9):17664–79.
48. Han X, Wu X, Liu F, Chen H, Hou H. Inhibition of LPS-induced inflammatory response in RAW264.7 cells by natural Chlorogenic acid isomers involved with AKR1B1 inhibition. Bioorg Med Chem. 2024 Nov;114:117942.
49. Kim SH, Park SY, Park YL, Myung DS, Rew JS, Joo YE. Chlorogenic acid suppresses lipopolysaccharide-induced nitric oxide and interleukin-1β expression by inhibiting JAK2/STAT3 activation in RAW264.7 cells. Mol Med Rep. 2017 Dec;16(6):9224–32.
50. Huang Q, Shan Q, Ma F, Li S, Sun P. Chlorogenic acid mitigates heat stress-induced oxidative damage in bovine mammary epithelial cells by inhibiting NF-κB-mediated NLRP3 inflammasome activation via upregulating the Nrf2 signaling pathway. Int J Biol Macromol. 2025 Apr;301:140133.
51. Petersen M, Abdullah Y, Benner J, Eberle D, Gehlen K, Hücherig S, et al. Evolution of rosmarinic acid biosynthesis. Phytochemistry. 2009 Oct;70(15–16):1663–79.
52. Lee J, Kim G. Evaluation of Antioxidant and Inhibitory Activities for Different Subclasses Flavonoids on Enzymes for Rheumatoid Arthritis. J Food Sci. 2010 Sep 22;75(7).
53. Sugahara Y, Komorisono M, Kuwajima M, Yoshikawa S, Yoshida S, Maeda K. Anti-skin-aging effects of human ceramides via collagen and fibrillin expression in dermal fibroblasts. Biosci Biotechnol Biochem. 2022 Aug 24;86(9):1240–6.
54. Casati S, Giannasi C, Niada S, Della Morte E, Orioli M, Brini AT. Lipidomics of Cell Secretome Combined with the Study of Selected Bioactive Lipids in an In Vitro Model of Osteoarthritis. Stem Cells Transl Med. 2022 Sep 21;11(9):959–70.
55. Li Y, Lei D, Swindell WR, Xia W, Weng S, Fu J, et al. Age-Associated Increase in Skin Fibroblast–Derived Prostaglandin E2 Contributes to Reduced Collagen Levels in Elderly Human Skin. Journal of Investigative Dermatology. 2015 Sep;135(9):2181–8.
56. Subbaramaiah K, Chung WJ, Dannenberg AJ. Ceramide Regulates the Transcription of Cyclooxygenase-2. Journal of Biological Chemistry. 1998 Dec;273(49):32943–9.
57. Merrill GF, Kurth EJ, Hardie DG, Winder WW. AICA riboside increases AMP-activated protein kinase, fatty acid oxidation, and glucose uptake in rat muscle. Am J Physiol Endocrinol Metab. 1997;273(6 36-6).
58. Holmes BF, Kurth-Kraczek EJ, Winder WW. Chronic activation of 5'-AMP-activated protein kinase increases GLUT-4, hexokinase, and glycogen in muscle. J Appl Physiol. 1999;87(5).
59. Abe D, Saito T, Nogata Y. Rosmarinic Acid Regulates Fatty Acid and Glucose Utilization by Activating the CaMKK/AMPK Pathway in C2C12 Myotubes. Food Sci Technol Res. 2016;22(6):779–85.
60. Naimi M, Vlavcheski F, Murphy B, Hudlicky T, Tsiani E. Carnosic acid as a component of rosemary extract stimulates skeletal muscle cell glucose uptake via <scp>AMPK</scp> activation. Clin Exp Pharmacol Physiol. 2017 Jan 27;44(1):94–102.
61. Eid HM, Thong F, Nachar A, Haddad PS. Caffeic acid methyl and ethyl esters exert potential antidiabetic effects on glucose and lipid metabolism in cultured murine insulin-sensitive cells through mechanisms implicating activation of AMPK. Pharm Biol. 2017 Jan 23;55(1):2026–34.
62. Piazzon A, Vrhovsek U, Masuero D, Mattivi F, Mandoj F, Nardini M. Antioxidant Activity of Phenolic Acids and Their Metabolites: Synthesis and Antioxidant Properties of

the Sulfate Derivatives of Ferulic and Caffeic Acids and of the Acyl Glucuronide of Ferulic Acid. J Agric Food Chem. 2012 Dec 19;60(50):12312–23.
63. Prabhakar PK, Doble M. Synergistic effect of phytochemicals in combination with hypoglycemic drugs on glucose uptake in myotubes. Phytomedicine. 2009 Dec;16(12):1119–26.
64. Singdam P, Naowaboot J, Senggunprai L, Boonloh K, Hipkaeo W, Pannangpetch P. The Mechanisms of Neochlorogenic Acid (3-Caffeoylquinic Acid) in Improving glucose and Lipid Metabolism in Rats with Insulin Resistance Induced by A High Fat-High Fructose Diet. Trends in Sciences. 2023 Jan 17;20(3):6455.
65. Foukas LC, Daniele N, Ktori C, Anderson KE, Jensen J, Shepherd PR. Direct Effects of Caffeine and Theophylline on p110δ and Other Phosphoinositide 3-Kinases. Journal of Biological Chemistry. 2002 Oct;277(40):37124–30.
66. Bollati C, Fanzaga M, d'Adduzio L, Lammi C. Molecular and Human In Vivo Study of an Innovative Plant-Derived Multifunctional Peptide Signaling the Collagen and Elastin Pathways and Melanin Production. Cosmetics. 2025 May 15;12(3):100.
67. Bi J, Jing H, Zhou C, Gao P, Han F, Li G, et al. Regulation of skeletal myogenesis in C2C12 cells through modulation of Pax7, MyoD, and myogenin via different low-frequency electromagnetic field energies. Technology and Health Care. 2022 Feb 25;30:371–82.
68. Zanoni C, Aiello G, Arnoldi A, Lammi C. Investigations on the hypocholesterolaemic activity of LILPKHSDAD and LTFPGSAED, two peptides from lupin β-conglutin: Focus on LDLR and PCSK9 pathways. J Funct Foods. 2017;32.

Figures and tables

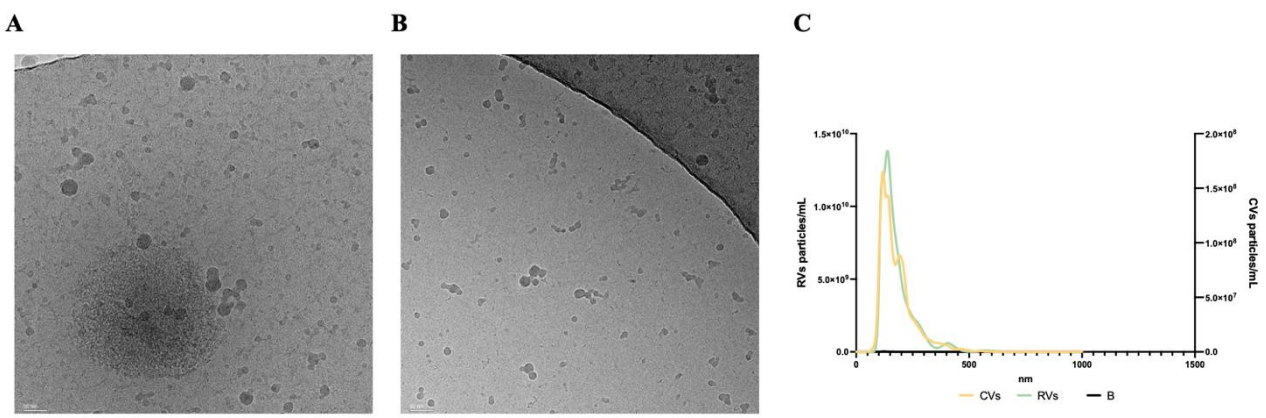

Figure 1 – **Cryogenic electron microscopy of CVs and RVs**. (A) Coffee-derived vesicles. (B) Rosemary-derived vesicles. Scale bar 50 nm for both the pictures. (C) NTA of CVs and RVs samples, respectively.

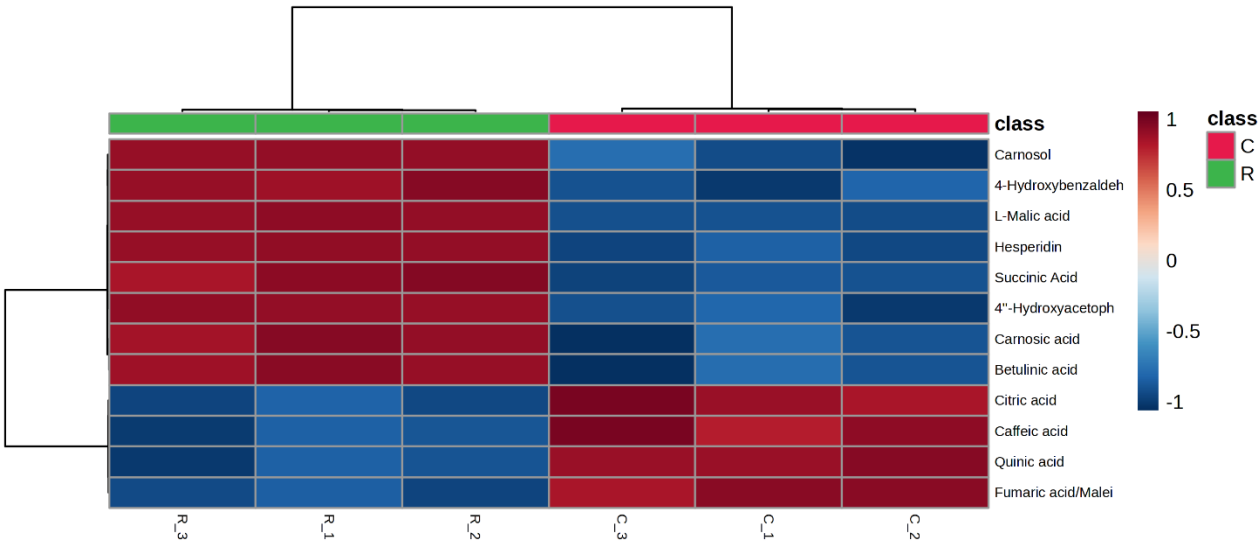

Figure 2 – Hierarchical clustering heatmaps of the relative abundance of common phytochemicals (one-way ANOVA and post-hoc analysis, $p < 0.05$) of CVs and RVs. More expressed phytochemicals are indicated in red, with intensity values represented by colored cells (red for higher expression and dark blue for lower expression); the samples are shown in the rows, and the features are shown in the columns.

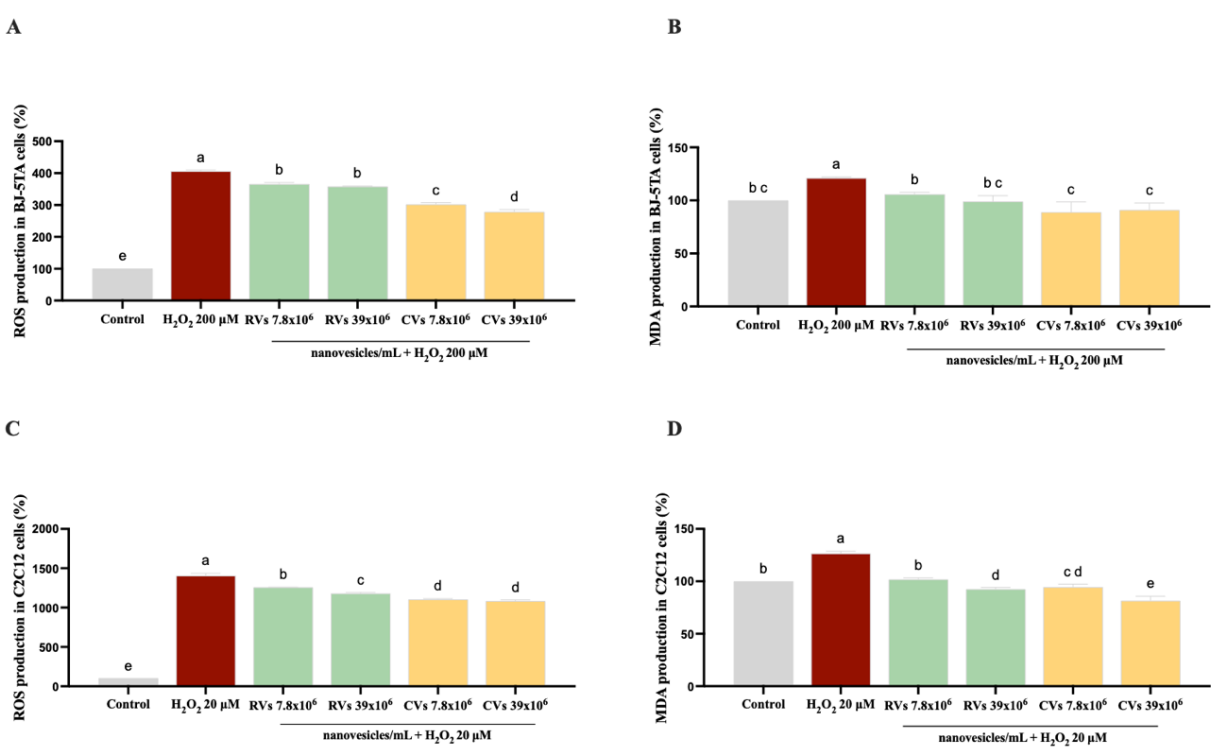

Figure 3 – RVs and CVs antioxidant activity. Evaluation of the effects of the RVs and CVs on H_2O_2 -induced reactive oxygen species (ROS) and MDA production levels in fibroblast BJ-5TA cells (A, B) and differentiated C2C12 (C, D) cells. The data points represent the averages ± SD of three independent experiments in duplicate. All data sets were analyzed by one-way ANOVA followed by Tukey's post hoc test. Different lowercase letters indicate a significant difference ($p < 0.05$) between different treatments. Control: untreated cells. RVs: rosemary vesicles; CVs: coffee vesicles. 7.8×10^6 vesicles/mL and 39×10^6 vesicles/mL correspond to 0.1 and 0.5 mg nanovesicles/mL.

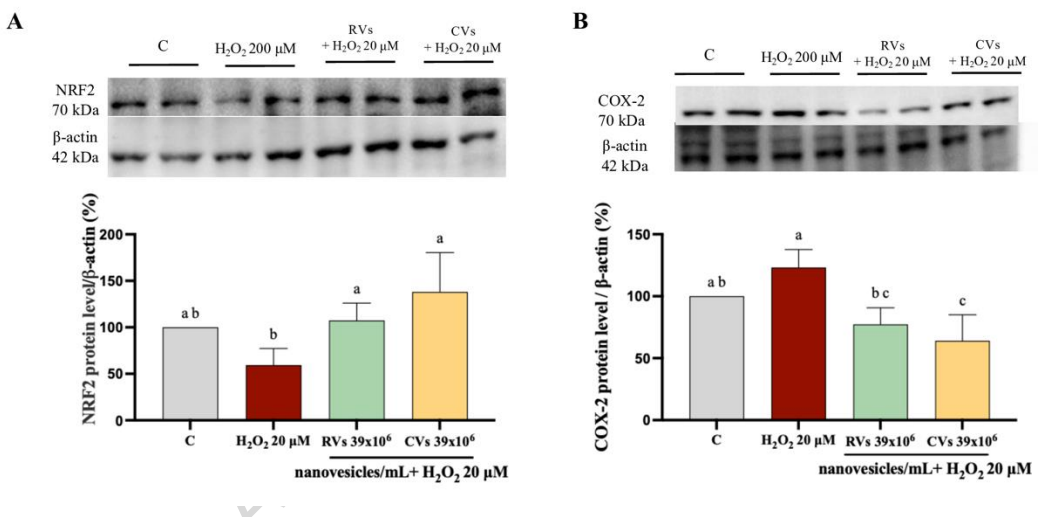

Figure 4 – Nrf2 and COX-2 protein levels in C2C12 cells pretreated with RVs and CVs $39x10^6$ vesicles/mL in oxidative stress induced damage. The data points represent the averages ± SD of three independent experiments in duplicate. All data sets were analyzed by one-way ANOVA followed by Tukey's post hoc test. Different lowercase letters indicate a significant difference ($p < 0.05$) between different treatments. Control: untreated cells. RVs: rosemary-derived vesicles; CVs: coffee-derived vesicles. 7.8×10^6 vesicles/mL and 39×10^6 vesicles/mL correspond to 0.1 and 0.5 mg nanovesicles/mL.

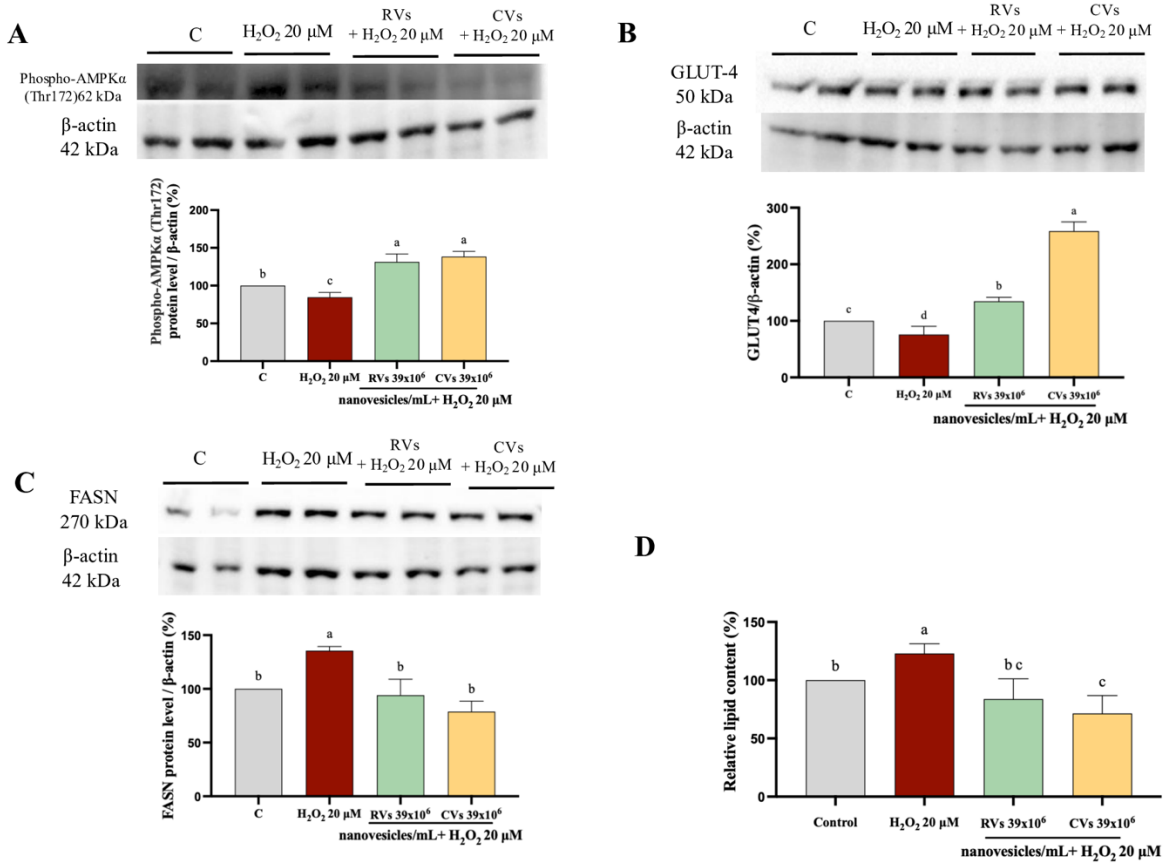

Figure 5 – pAMPK, FASN and GLUT4 protein levels and quantification of intracellular lipid accumulation in C2C12 cells pretreated with RVs and CVs 39x10^6 vesicles/mL in oxidative stress induced damage. The data points represent the averages ± SD of three independent experiments in duplicate. All data sets were analysed by one-way ANOVA followed by Tukey's post hoc test. Different lowercase letters indicate a significant difference ($p < 0.05$) between different treatments. Control: untreated cells. RVs: rosemary-derived vesicles; CVs: coffee-derived vesicles. pAMPK: AMP-activated protein kinase; GLUT-4: Glucose Transporter; FASN: Fatty Acid Synthase. 7.8×10^6 vesicles/mL and 39×10^6 vesicles/mL correspond to 0.1 and 0.5 mg nanovesicles/mL.

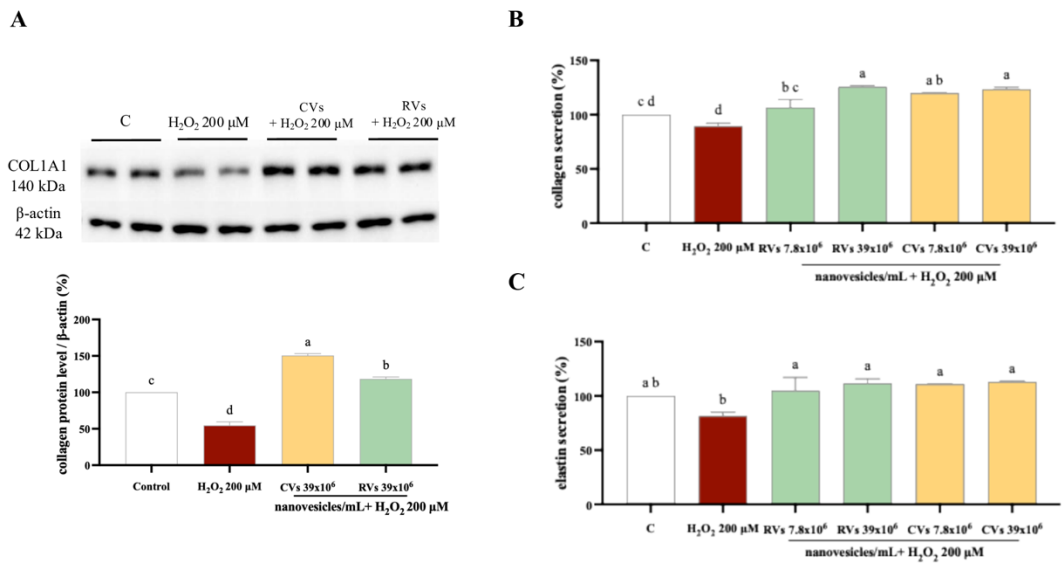

Figure 6 – Impact of CVs and RVs on collagen synthesis and collagen and elastin extracellular release. Collagen protein levels (A) and collagen and elastin secretion in human fibroblasts pretreated with RVs and CVs 39x10^6 nanovesicles/mL in oxidative stress induced damage (B, C). The data points represent the averages ± SD of three independent experiments in duplicate. All data sets were analyzed by one-way ANOVA followed by Tukey's post hoc test. Different lowercase letters indicate a significant difference ($p < 0.05$) between different treatments. Control: untreated cells. RVs rosemary-derived vesicles; CVs: coffee-derived vesicles. 7.8×10^6 vesicles/mL and 39×10^6 vesicles/mL correspond to 0.1 and 0.5 mg nanovesicles/mL.

Table 1 – Dynamic Light Scattering and Nanoparticle Tracking Analysis results of CVs and RVs. Results are expressed as the mean ± s.d. (n=3).

Sample	Angle (°)	DLS						NTA				
		Dh (nm)		PDI		DCR (kcps)		D10	D50	D90	#/mL	
CVs	173°	300	15	0,351	0,061	5473	207	109,3	159,2	277	1,74E+10	4,34E+08
	12,8°	593	69	0,923	0,134	6052	1077					
RVs	173°	222	25	0,479	0,059	16702	150	112,6	156,1	268,9	1,37E+12	3,23E+10
	12,8°	565	74	0,251	0,226	10124	1388					

DLS = Dynamic Light Scattering; NTA = Nanoparticle Tracking Analysis; D_h = Z-average diameter; PDI = Polydispersity Index.